International Journal Of
Industrial Electronics Control and Optimization
Print ISSN: 3517-2645
Online ISSN: 3568-2645
Homepage: https://ieco.usb.ac.ir/

A State-of-Charge fusion estimation of Lithium-Ion batteries based on the mathematical models of the open circuit voltage curve

Mohammad Moodi[1] | Mohammad Reza Ramezani-al[2]

Department of Electrical Engineering, Faculty of Electrical and Computer Engineering, Quchan University of Technology, Quchan, Iran.[1,2]
Corresponding author's email: m-ramezani@qiet.ac.ir

Article Info

Article type:
Research Article

Article history:
Received: **********
Received in revised form: **********
Accepted: **********
Published online: **********

Keywords:
Fusion estimation,
Lithium-Ion battery,
OCV-SOC curve,
State-of-charge.

ABSTRACT

Accurate state-of-charge (SOC) estimation is essential for the safe and efficient operation of lithium-ion batteries in electric vehicles and energy storage systems. This paper proposes a fusion-based SOC estimation method that integrates two extended Kalman filters (EKFs), each paired with a distinct open-circuit voltage (OCV)–SOC model. The fusion strategy, grounded in Bayesian probability and residual error analysis, dynamically assigns weights to each model's output, ensuring that the most appropriate model contributes predominantly to the final SOC estimate at any given moment. The proposed framework utilized a second-order equivalent circuit model (ECM) and estimates parameters online via a variable forgetting factor recursive least squares (VFFRLS) algorithm. Simulation results under LA92 and UDDS driving cycles demonstrate that the method achieves superior accuracy and robustness, reducing the maximum estimation error by up to 26% and RMSE by over 10% compared to conventional EKF approaches. These findings highlight the method's effectiveness and adaptability for real-time battery management applications.

I. Introduction

In response to global energy constraints and the accelerating shift toward low-carbon technologies, lithium-ion batteries have become indispensable across a wide range of applications, including electric vehicles (EVs), consumer electronics, and renewable energy systems [1], [2]. Their high energy density, long cycle life, and rapid charging capabilities make them ideal for modern energy storage [3], [4]. Central to effective battery management is accurate estimation of the SOC, which reflects the remaining capacity of a battery relative to its full charge. SOC estimation is critical for ensuring safety, optimizing performance, and extending battery lifespan [5], [6].

Recent literature classifies SOC estimation techniques into two categories: direct and indirect. Among direct methods, the Coulomb Counting (CC) approach is widely adopted for its simplicity [7]. However, its reliance on the initial SOC value and open-loop design often causes error accumulation [8]. To address these issues, indirect methods have gained prominence and are further divided into adaptive filters and artificial intelligence (AI) techniques. AI approaches, such as recurrent neural networks (RNN) [9], feed-forward neural networks (FNN) [10], and support vector machines (SVM) [11], leverage experimental data to model the nonlinear relationship between SOC and external parameters. Despite their accuracy, AI methods require extensive data and computational resources, which limits their practical applicability. On the other hand, adaptive filter-based techniques strike a balance between simplicity and accuracy, making them cost-effective and suitable for resource-limited embedded systems. These methods involve selecting a battery model and determining its parameters, deriving the OCV-SOC relationship, and designing a state estimation algorithm.

Over the past decade, researchers have developed a range of adaptive filter algorithms to improve the accuracy and robustness of battery state estimation. Among these, the Kalman filter (KF) family—including the EKF, unscented Kalman filter (UKF), and cubature Kalman filter (CKF)—

Copyright © Author(s).
Publisher: University of Sistan and Baluchestan

has been widely adopted due to its balance of computational efficiency and estimation performance [5], [12], [13]. Other methods, such as H∞ filters and RLS, have also been explored. While RLS is effective for parameter identification in ECM, it struggles with divergence in nonlinear systems [12]. The H∞ filter offers robustness under uncertainty[14], but introduces significant computational complexity, making it less suitable for embedded applications with limited resources. Among these, EKF remains a preferred choice for SOC estimation due to its simplicity and adaptability to nonlinear battery dynamics [15]. However, even the most refined filtering algorithms face limitations when applied uniformly across different operating conditions.

To address these limitations, fusion techniques have emerged as a powerful solution for enhancing SOC estimation accuracy and robustness. Battery behavior is inherently nonlinear and varies across discharge intervals due to electrochemical dynamics, temperature effects, and aging. A single model or algorithm may perform well in one interval but poorly in others. Fusion methods allow the integration of multiple models and algorithms, each selected based on its performance in specific operating conditions. This approach not only improves estimation accuracy but also enhances generalizability across battery types and environments. Moreover, fusion techniques can mitigate noise sensitivity and provide smoother outputs, making them particularly valuable for real-world applications such as electric vehicles and energy storage systems.

In recent years, fusion-based SOC estimation techniques have gained prominence for their ability to combine the strengths of multiple models and algorithms. For instance, Wu et al. [16] proposed a multidimensional element space mapping architecture (MESMA) that integrates an ECM with convolutional neural networks (CNN) and XGBoost, achieving high adaptability across temperatures but introducing computational complexity. Cheng et al. [17] introduced a three-interval fusion approach for SOC estimation, leveraging fitness-based model-algorithm selection to enhance accuracy. Zhou et al. [18] presented a hybrid MIEKPF-EKPF algorithm for SOC and state of health (SOH) estimation in Lithium-ion batteries, integrating multi-innovation theory with extended Kalman particle filtering. By compensating for aging effects and leveraging past observations, it achieves high accuracy. Li et al. [19] introduced a multi-model fusion framework using Thevenin and second-order ECMs, UKF, and Bayesian weighting, achieving SOC estimation errors within 1% and incorporating fault diagnosis via residual innovation sequences. Chen et al. [20] developed a multi-task learning network for simultaneous SOC and state of energy (SOE) estimation using multi-layer feature extraction and expert layers, offering high fusion accuracy but remaining sensitive to input noise. Collectively, these studies underscore the potential of fusion-based SOC estimation to enhance precision, fault tolerance, and adaptability. Despite these advancements, fusion methods often face challenges related to computational complexity, model transparency, and real-time applicability.

The OCV-SOC relationship in lithium-ion batteries is influenced by several factors, including temperature, aging, and discharge rate. Accurate SOC estimation hinges on the ability to model this nonlinear curve effectively, as it directly impacts the reliability of model-based predictions. Consequently, the mathematical formulation used to represent the OCV-SOC relationship plays a critical role in determining estimation accuracy. In most existing literature, this curve is approximated using polynomial, exponential, or piecewise functions [13], [21], [22]. However, a single model often fails to capture the full spectrum of nonlinear behavior across varying operating conditions, limiting its generalizability and precision.

To address this issue, this paper introduces a fusion estimation method based on the EKF to enhance the accuracy of SOC estimation under diverse operating conditions. The proposed algorithm significantly improves robustness, effectiveness, and reliability while maintaining computational simplicity—unlike conventional fusion strategies that often involve complex switching logic and high processing demands. In this method, two optimal mathematical models are independently selected from a set of seven well-established OCV-SOC models in the literature, based on error analysis. These models are embedded into two separate ECMs, each integrated with its own EKF algorithm, resulting in two distinct SOC estimations at each time step. Additionally, the RLS algorithm with a variable forgetting factor is employed to estimate ECM parameters online. The final SOC value is obtained by fusing the two estimations, with fusion weights determined by the statistical characteristics of the residual error in terminal voltage (RETV), thereby enhancing overall accuracy and reliability.

The remainder of the paper is organized as follows: Section 2 introduces the selected ECM and derives the governing equations for its parameters. Section 3 presents the proposed fusion algorithm in detail. Section 4 provides simulation results and evaluates the performance of the proposed method alongside benchmark algorithms. Finally, Section 5 concludes the paper with final remarks and potential directions for future research.

II. Battery modeling and parameter identification algorithm

A. Battery model

The accuracy of the battery model significantly affects the precision of SOC estimation algorithms, but computational constraints in industrial applications necessitate a balance between simplicity and accuracy [23]. Lithium-ion battery models are generally categorized into ECMs[24], data-driven AI models [25], and electrochemical models [26].

ECMs are widely used due to their ease of implementation [27], reasonable computational burden [2], and adequate accuracy, making them suitable for online applications. A review of eleven ECMs identifies first-order (1RC) and second-order (2RC) RC models as the most reliable and accurate [28]. The 1RC model, while less complex, struggles in dynamic situations, whereas the 2RC model performs better under varying currents and C-rates, making it ideal for applications such as laptops and electric vehicles [29]. Based on this, the proposed algorithm in this paper was tested under highly dynamic scenarios, with the 2RC model selected to effectively represent battery behavior.

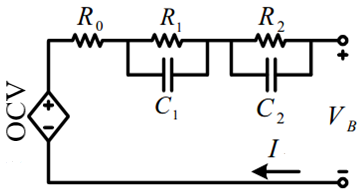

Fig. 1. The 2RC model of the lithium-ion battery

In the 2RC model, the OCV represents the battery's terminal voltage when it reaches internal equilibrium with zero load current. The internal resistance (R_0), terminal voltage ($V_B(t)$), and polarization states (R_1, C_1, R_2, C_2) are parameters used to describe the battery's internal electrochemical behavior. Based on Fig. 1 and basic circuit principles, the mathematical expressions for the 2RC model are derived as follows:

$$\begin{cases} C_1 \dfrac{dV_1(t)}{dt} + \dfrac{V_1(t)}{R_1} = I(t) \\ C_2 \dfrac{dV_2(t)}{dt} + \dfrac{V_2(t)}{R_2} = I(t) \end{cases} \tag{1}$$

So, we have:

$$\begin{cases} \dot{V}_1(t) = -\dfrac{V_1(t)}{R_1C_1} + \dfrac{I(t)}{C_1} \\ \dot{V}_2(t) = -\dfrac{V_2(t)}{R_2C_2} + \dfrac{I(t)}{C_2} \\ V_B(t) = OCV(t) - R_0I(t) - V_1(t) - V_2(t) \end{cases} \tag{2}$$

The discretized form of the 2RC model is given by:

$$\begin{cases} V_1(k+1) = V_1(k)e^{-\frac{T_s}{R_1C_1}} + I(k)R_1\left(1 - e^{-\frac{T_s}{R_1C_1}}\right) \\ V_2(k+1) = V_2(k)e^{-\frac{T_s}{R_2C_2}} + I(k)R_1\left(1 - e^{-\frac{T_s}{R_2C_2}}\right) \\ V_B(k) = OCV(k) - R_0I(k) - V_1(k) - V_2(k) \end{cases} \tag{3}$$

where, T_s is the sampling time and k and $k+1$ represent the consequence times.

B. Parameter identification

Model parameters can be estimated online or offline, with online estimation being more precise due to variations in temperature, SOC, and other factors. The RLS algorithm is a well-known method for estimating battery parameters and is easy to implement online [30], [31]. However, its accuracy diminishes with increasing data volumes. To address this, a forgetting factor (FF) is used to prioritize new data, but a constant FF is unsuitable for varying conditions. Therefore, the variable forgetting factor RLS (VFFRLS) algorithm is applied in this paper to estimate the 2RC model's parameters online, accommodating time-varying conditions. Suppose at sampling time k, system output is written as:

$$Y(k) = \phi(k)\theta(k)^T + \varepsilon(k) \tag{4}$$

Where $\phi(k)$ represents the vector of known information, $\theta(k)$ denotes the vector of unknown parameters, $Y(k)$ is the system's output, and $\varepsilon(k)$ is random noise. The primary equations of the RLS algorithm with a forgetting factor are:

$$\begin{cases} K(k) = -\dfrac{P(k-1)\phi(k)}{\lambda + \phi(k)^T P(k-1)\phi(k)} \\ e(k) = Y(k) - \phi(k)^T\theta(k-1) \\ \theta(k) = \theta(k-1) + K(k)e(k) \\ P(k) = \dfrac{1}{\lambda}(I - K(k)\phi(k)^T)P(k-1) \end{cases} \tag{5}$$

Where $K(k)$ is the estimator gain, $P(k)$ is the covariance matrix, $e(k)$ is the error vector, and λ is the forgetting factor. The variable forgetting factor λ(k) is selected at each sampling time using the following rule [32]:

$$\lambda(k) = \begin{cases} \lambda_{max}; (0 < |e(k)| < 0.005) \\ \lambda_{max} - (\lambda_{max} - \lambda_{min})\left(\dfrac{|e(k)|}{e_{max}}\right)^2; (0.005 < |e(k)| < 0.05) \\ \lambda_{min} = V_B(k); \text{ for } |e(k)| \geq 0.05 \end{cases} \tag{6}$$

The value of e_{max} is considered 0.01 and generally $0.95 < \lambda < 1$. Using measured data at each sampling time and the VFFRLS algorithm, all model parameters are identified online.

C. OCV-SOC Curve's Mathematical Models

The relationship between OCV and SOC in lithium-ion batteries is inherently nonlinear and is typically characterized through offline experimental measurements. To model this behavior, a variety of mathematical functions including high-order polynomials (commonly 7th), logarithmic, exponential, and hybrid formulations have been proposed, each offering distinct advantages and limitations [13]. Table I summarizes representative OCV–SOC models frequently cited in the literature, reflecting a range of strategies for capturing this nonlinear behavior.

Rational and logarithmic models (e.g., Models 1 and 6) are particularly effective near SOC boundaries but may introduce singularities at low SOC values. High-order polynomial models (Model 2) provide strong curve-fitting capabilities; however they are prone to overfitting and can become unstable outside the calibration range. Exponential models (Model 3) can represent steep voltage transitions, though they require careful parameter tuning. Sinusoidal models (Model 4) may capture subtle voltage oscillations,

though they lack physical interpretability in battery systems. Gaussian-like models (Model 5) provide localized fitting and smooth transitions, but their performance can be sensitive to the choice of initial parameters. Ultimately, the accuracy and suitability of each model depend on the specific battery chemistry, design, desired precision, computational constraints, and application context. These models are further evaluated based on their accuracy in Section 4.

TABLE I OCV-SOC Mathematical models in literature

num	Mathematical Model	Reference
1	$OCV = K_0 + K_1 SOC + \frac{K_2}{SOC} + K_3 \ln(SOC) + K_4 \ln(1 - SOC)$	[33]
2	$OCV = K_1 SOC^7 + K_2 SOC^6 + K_3 SOC^5 + K_4 SOC^4 + K_5 SOC^3 + K_6 SOC^2 + K_7 SOC + K_8$	[13]
3	$OCV = K_1 e^{\alpha 1.SOC} + K_2 e^{\alpha 2.SOC} + K_3 SOC^2$	[22]
4	$OCV = K_1 \sin(\alpha_1 SOC + \beta_1) + K_2 \sin(\alpha_2 SOC + \beta_2) + K_3 \sin(\alpha_3 SOC + \beta_3)$	[21]
5	$OCV = K_1 e^{\left(\frac{SOC-\alpha_1}{\beta_1}\right)^2} + K_2 e^{\left(\frac{SOC-\alpha_2}{\beta_2}\right)^2} + K_3 e^{\left(\frac{SOC-\alpha_3}{\beta_3}\right)^2}$	[21]
6	$OCV = K_0 + \frac{K_1}{SOC} + \frac{K_2}{SOC^2} + \frac{K_3}{SOC^3} + \frac{K_4}{SOC^4} + K_5 SOC + K_6 \ln(SOC)$	[34]

III. SOC estimation algorithms

A. SOC estimation by EKF method

The KF is a commonly used tool for estimating dynamic system states across various industries. Its nonlinear variant, the EKF, is widely utilized for battery SOC estimation. The EKF algorithm is implemented using the discrete state equations of the battery model, which are provided in Eq. 7.

$$\begin{cases} \begin{bmatrix} SOC(k+1) \\ V_1(k+1) \\ V_2(k+1) \end{bmatrix} = \begin{bmatrix} 1 & 0 & 0 \\ 0 & e^{\frac{-\Delta t}{R_1 C_1}} & 0 \\ 0 & 0 & e^{\frac{-\Delta t}{R_2 C_2}} \end{bmatrix} \begin{bmatrix} SOC(k) \\ V_1(k) \\ V_2(k) \end{bmatrix} + \begin{bmatrix} \frac{\Delta t}{C_{bat}} \\ R_1\left(1 - e^{\frac{-\Delta t}{R_1 C_1}}\right) \\ R_2\left(1 - e^{\frac{-\Delta t}{R_2 C_2}}\right) \end{bmatrix} . I(k) + \omega(k) \\ V_B(k) = \begin{bmatrix} \frac{dOCV(soc(k))}{dSOC(k)} & -1 & -1 \end{bmatrix} \begin{bmatrix} SOC(k) \\ V_1(k) \\ V_2(k) \end{bmatrix} - R_0 I(k) + \nu(k) \end{cases} \quad (7)$$

In Eq. (7), the battery current $I(k)$ and terminal voltage $V_B(k)$ are considered as the input and output of the system, respectively. The state vector is defined as $[SOC, V_1, V_2]$, where V_1 and V_1 represent the voltages across the RC blocks. The term $\omega(k)$ denotes the stochastic process noise, which is unmeasurable and affects the system states, while $\nu(k)$ represents the measurement noise. Also, Δt is the sampling interval, and C_{bat} is the battery capacity. Fig. 2 demonstrates the SOC estimation process using the EKF algorithm.

At each sampling interval, battery voltage and current are measured, and battery parameters are determined via the VFFRLS technique and battery equations. Then, the SOC is estimated using the EKF algorithm and the OCV-SOC model (Eq. 7). Finally, accuracy is verified by comparing the estimated SOC with experimental values obtained through the CC method.

B. SOC estimation with proposed fusion method

Model-based SOC estimation of lithium-ion batteries requires the mathematical representation of the OCV-SOC curve and its variation with respect to SOC, i.e., $\frac{\mathrm{dOCV(soc(k))}}{\mathrm{dSOC(k)}}$, as described in the state space equations (Eq. 7). Although polynomial functions are commonly used in the literature to model this curve, they cannot account for all situations and working conditions. This paper proposes a fusion SOC estimation process that employs two EKF algorithms simultaneously, each utilizing a different mathematical model from Table 1 to represent the OCV-SOC curve. The final SOC is calculated as a linear combination of the two SOC estimates at each sampling time, as shown in Eq. 8.

$$\begin{cases} SOC_f(k) = W_1(k) SOC_1(k) + W_2(k) SOC_2(k) \\ W_1(k) + W_2(k) = 1 \end{cases} \quad (8)$$

Where, $SOC_1(k)$ and $SOC_2(k)$ are the estimated SOCs using each EKF, $W_1(k)$ and $W_2(k)$ are the weights of each estimation, and $SOC_f(k)$ is the final fusion estimation value. Fig. 3 illustrates SOC estimation in the proposed fusion method.

In the proposed fusion estimation method, determining the weight of each SoC estimate at every sampling time is essential. The RETV serves as a key metric for evaluating the accuracy of SoC estimations produced by each EKF estimator [33], [35]. The weight assigned to each estimate is inversely related to its RETV (higher error leads to lower weight, and vice versa). This relationship is expressed as:

$$r_i(k) = V_B(k) - \hat{V}_{Bi}(k) \quad (9)$$

where $V_B(k)$ is the measured terminal voltage and $\hat{V}_{Bi}(k)$ is the voltage estimated by the ith EKF.

However, RETV alone is insufficient for robust accuracy assessment in parallel algorithms. To enhance its reliability, we incorporate statistical properties of RETV into the weight calculation. Assuming RETV follows a normal distribution, Bayes' theorem is applied to derive a conditional probability density function (PDF) for each estimator at time k:

$$f(V_B(k)|p_i) = \frac{1}{\sqrt{2\pi S_i(k)}} \exp\left(-\frac{1}{2}\ \bar{r}_i^2(k) S_i(k)\right) \quad (10)$$

Where:

$$\begin{cases} \bar{r}_i(k) = \frac{1}{L_m} \sum_{j=k-L_m+1}^{k} r_{ij} \\ S_i(k) = \frac{1}{L_m} \sum_{j=k-L_m+1}^{k} \left(r_{ij} - \bar{r}_{ik}\right)^2 \end{cases} \quad (11)$$

Here, p_i denotes the parameter set of the ith EKF estimator, and $\bar{r}_i(k)$ and $S_i(k)$ represent the mean and variance of

RETV over a sliding window of length L_m.The shape of the likelihood function is directly influenced by these RETV statistics: A lower mean error and variance result in a sharper, higher peak in the probability density function (PDF), indicating greater confidence in the estimator. Conversely, a higher mean or variance produces a flatter, lower peak, reflecting reduced reliability.

This probabilistic interpretation enables the fusion algorithm to dynamically favor estimators that demonstrate more consistent and accurate performance.

The value of L_m has a significant impact on the algorithm's performance. While increasing the length of L_m can improve accuracy, it also increases computational cost. Therefore, the optimal L_m should be chosen by balancing these two factors. Table VI presents the results, showing how different L_m values affect both the average computation time and SoC estimation accuracy. According to the data, when $L_m$exceeds 400, there is no further improvement in accuracy—only an increase in computation time. Considering this trade-off, a length of 300 was chosen for L_m in this study.

For sampling times $k < L_m$, the values of $\bar{r}_i(k)$ and $S_i(k)$ are initialized to one to ensure stability during startup. Finally, the weight for each estimator is computed using the normalized posterior probability:

$$W_i(k) = P(p_i|V_B(k)) = \left(1 - \frac{f(V_B(k)|p_i)S_i(k)}{\sum_{j=1}^{2} f(V_B(k)|p_j)S_j(k)}\right) \quad (12)$$

This fusion strategy enhances the baseline SoC estimation algorithm (Section 3.1) by improving accuracy, robustness, and reliability with minimal additional computational load.

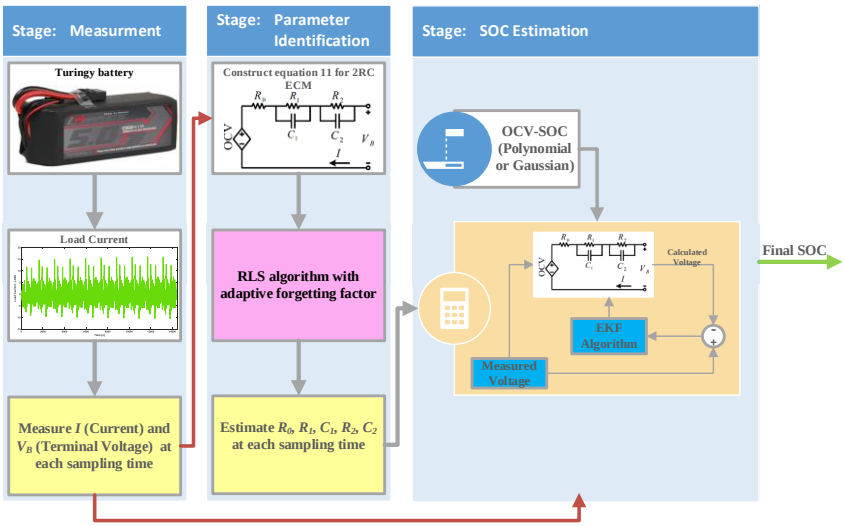

Fig. 2. SOC estimation scheme with EKF

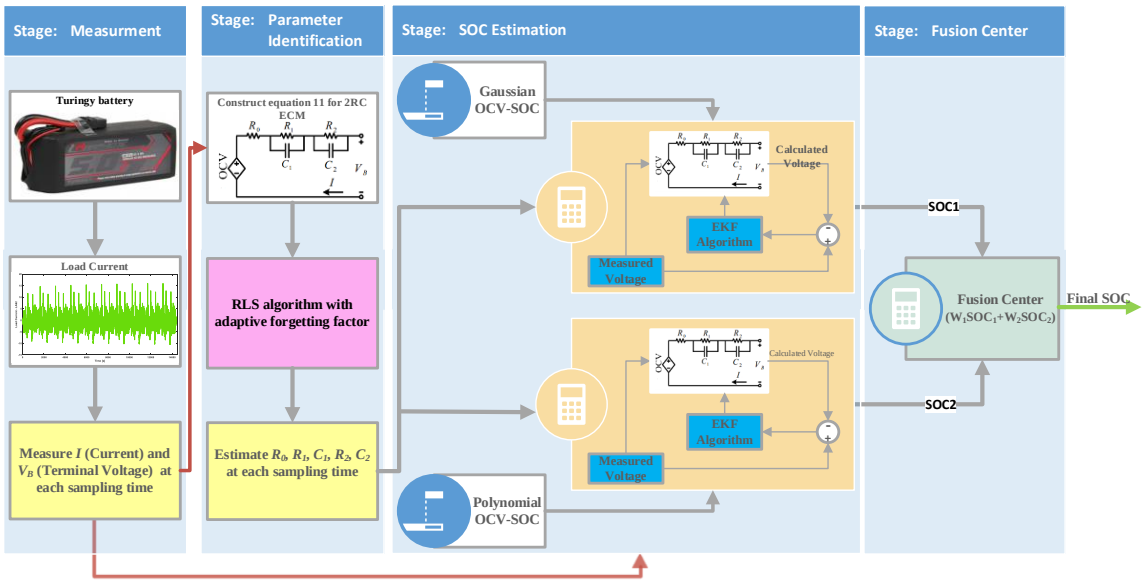

Fig. 3. SOC estimation scheme with proposed fusion algorithm

IV. Experimental Results

A. Battery data

In this section, the practical measured voltage and current of the new Turingy Graphene 5000mAh 65C battery during the LA-92 test are used to simulate and evaluate the proposed method and compare it with other methods. In addition, all the results have been obtained under the UDDS test. The main characteristics of the battery are shown [36].

TABLE II Battery specification of Turingy Graphene 5000mAh 65C

Chemistry	LiPO
Nominal Voltage	3.7 V
Charge	4.2V, 50mA End-Current (CC-CV) Fast
Discharge	2.8V End Voltage, 20A MAX Continuous Current
Nominal Capacity	5 Ah
Energy Density	134 (Wh/Kg)

The LA-92 and UDDS dynamic driving cycles at 25°C are chosen to evaluate the SOC estimation methods and to prove the effectiveness of the proposed method. These tests consider harsh dynamic conditions for the battery and include continuous and back-to-back charging and discharging. In addition, the C-Rate is also variable. For example, it increases up to 3C in LA-92 test. The battery current and voltage diagram during these tests is shown in Fig. 4.

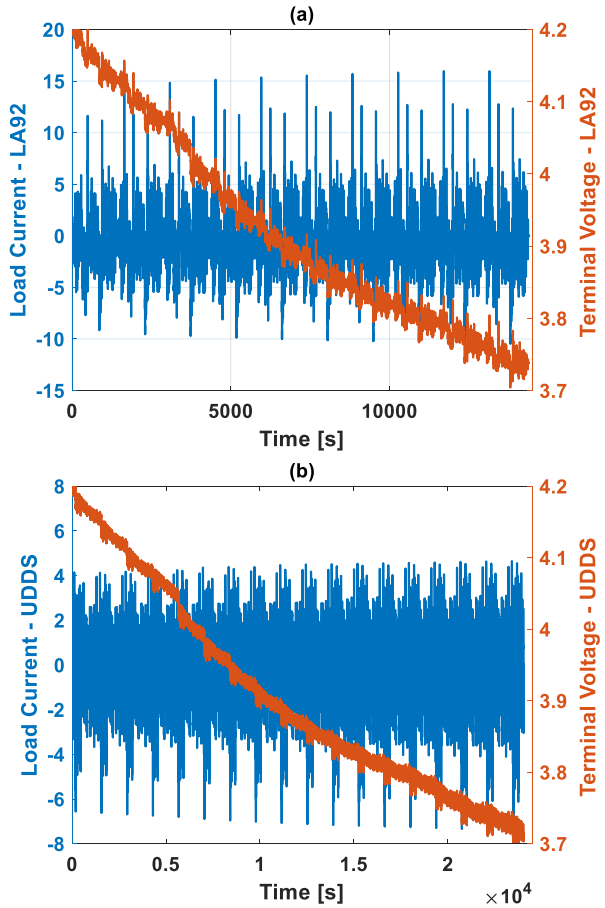

Fig. 4. Load Current and Terminal Voltage Profiles During LA92 and UDDS Driving Cycles. Figure (a) shows the LA92 cycle, where the load current exhibits sharp fluctuations, simulating aggressive acceleration and braking patterns. The terminal voltage gradually decreases. Figure (b) presents the UDDS cycle, characterized by frequent changes in load current. Both cycles impose harsh dynamic conditions on the battery, providing a rigorous test environment for evaluating its performance and durability.

Using MATLAB, six mathematical models (listed in Table 1) were fitted to 12 data points extracted from the experimentally obtained OCV-SOC curve of the Turingy Graphene 5000 mAh 65C battery. The resulting RMSE values from the fitting process are summarized in Table III.

TABLE III RMSE value of fitted curve

Model	**1**	**2**	**3**	**4**	**5**	**6**
RMSE	0.01281	0.0111	0.0327	0.0332	0.0036	0.0114

Models 3 and 4 exhibited the highest RMSE values, indicating poor accuracy for this specific battery type. Although Models 1 and 6 showed acceptable accuracy, their mathematical structures involve singularities and logarithmic terms that complicate derivative computation and may introduce instability in the estimation algorithm. To ensure compatibility with the SOC estimation framework (Eq. 5), the selected models must support both the mathematical expression and its derivative, i.e., $\frac{dOCV(soc(k))}{dSOC(k)}$. Based on a balance of fitting accuracy, analytical tractability, and numerical stability, Models 2 and 5 were chosen for implementation. Model 2 offers a smooth polynomial structure with straightforward differentiation, while Model 5 provides a flexible Gaussian formulation that captures nonlinear behavior effectively. These two models were selected for further integration into the SOC estimation framework.

To further evaluate the reliability and robustness of the selected polynomial and Gaussian models, a detailed sensitivity analysis was conducted. Each model was calibrated using experimental OCV data, and its parameters were individually perturbed by ±5% and ±10% to assess the impact on RMSE. As summarized in Table IV and Table V, which present the RMSE variation ranges and sensitivity levels for the polynomial and Gaussian models, respectively, the polynomial model exhibits a broad range of sensitivity. Specially coefficients K_2–K_5 showed high RMSE variation, indicating a strong influence on model accuracy, while parameters K_7 and K_8 had minimal impact. In contrast, the Gaussian model displayed distinct sensitivity patterns. Parameters govering the center and width of the dominant peak (notably β_1 and c_1) had the greatest effect on RMSE, while parameters associated with secondary peaks (α_3–c_3) contributed minimally, indicating limited influence on overall model performance. This analysis highlights the nuanced behavior of Gaussian model suggesting that careful tuning of its primary peak parameters is crucial for optimal

Copyright © Author(s).
Publisher: University of Sistan and Baluchestan

performance. For polynomial model, attention to its middle-order coefficients is essential to maintain accuracy.

TABLE IV RMSE variation and sensitivity levels for polynomial model parameters under ±5% and ±10% perturbations.

p	±5% RMSE Range	±10% RMSE Range	Sensitivity Level
K_1	3.3796 – 3.402	6.7705 – 6.7929	Moderate
K_2	14.479 – 14.502	28.969 – 28.992	High
K_3	25.453 – 25.476	50.918 – 50.941	Very High
K_4	23.763 – 23.786	47.538 – 47.560	Very High
K_5	12.73 – 12.752	25.471 – 25.494	High
K_6	3.9367 – 3.9584	7.8843 – 7.906	Moderate
K_7	0.67946 – 0.69922	1.3687 – 1.3885	Low
K_8	0.11387 – 0.12761	0.23383 – 0.24762	Very Low

TABLE V RMSE variation and sensitivity levels for Gaussian model parameters under ±5% and ±10% perturbations

P	±5% RMSE Range	±10% RMSE Range	Sensitivity Level
K_1	0.13749 – 0.13772	0.27508 – 0.27531	High
α_1	0.18874 – 0.19105	0.37383 – 0.38222	Very High
β_1	0.11463 – 0.12261	0.22189 – 0.25279	High
K_2	0.075674 – 0.075951	0.15145 – 0.15173	Moderate
α_2	0.0042117 – 0.0044886	0.0079751 – 0.0082758	Low
β_2	0.05947 – 0.061608	0.11695 – 0.12481	Moderate
K_3	0.0022864 – 0.0023797	0.0034087 – 0.0035342	Very Low
α_3	0.0047283 – 0.0049324	0.0088647 – 0.0096019	Low
β_3	0.0022384 – 0.0022622	0.0031861 – 0.0032922	Very Low

Figure 5 shows experimental OCV-SOC data and its approximations with polynomial and Gaussian models.

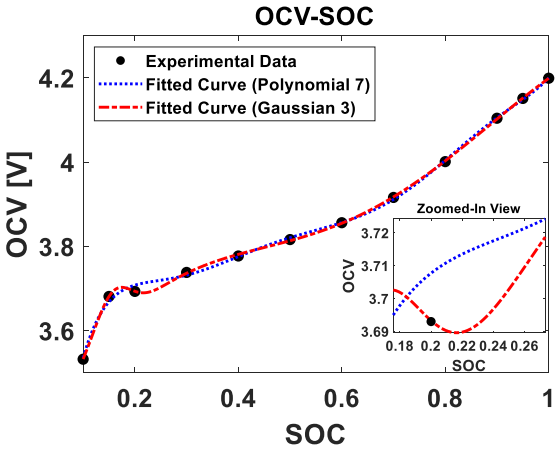

Fig, 5. Comparison of Polynomial and Gaussian fitting methods for OCV-SOC. Experimental data (black dots) are approximated using a 7th-order polynomial and a 3th-order Gaussian model. The inset zooms into the SOC range 0.18–0.26, highlighting subtle differences in curve behavior critical for battery performance modeling.

B. Performance evaluation indices

The study evaluates the proposed approach using error metrics such as Maximum Error (MAX), Mean Square Error (MSE), Root Mean Square Error (RMSE), and Mean Absolute Error (MAE). These metrics respectively measure reliability, robustness, and accuracy of the estimation method. Equation (11) contains the mathematical expressions for these criteria.

$$\begin{cases} MAE = \frac{1}{n}\sum_{k=1}^{n}\left|SOC_k - \widehat{SOC}_k\right| \\ MSE = \frac{1}{n}\sum_{k=1}^{n}\left(SOC_k - \widehat{SOC}_k\right)^2 \\ RMSE = \sqrt{\frac{1}{n}\sum_{k=1}^{n}\left(SOC_k - \widehat{SOC}_k\right)^2} \\ MAX = max\left|SOC_k - \widehat{SOC}_k\right| \end{cases} \quad (13)$$

C. Results and discussion

The SOC estimation results obtained using the EKF method during the LA-92 test are illustrated in Fig. 6. Specifically, Fig. 6(a) displays the SOC estimation outcomes for the 7th polynomial model and the 3rd Gaussian model, while Fig. 6(b) focuses on the corresponding estimation errors for these models. Notably, during certain intervals, such as from 8000 to 12000, the 7th polynomial model exhibits higher errors, whereas the 3rd Gaussian model demonstrates lower errors. Despite these differences, both models achieve acceptable accuracy, and the proposed approach combines their strengths to enhance overall performance.

The SOC estimation results and corresponding errors obtained through the proposed method during the LA-92 test are illustrated in Fig. 7. This approach combines two algorithms, resulting in improved overall estimation accuracy. As shown in Figure 7(b), the error range is narrower compared to the individual methods, highlighting enhanced performance throughout the test. Also, the resulting dynamic weights used in fusion are shown in Figure 8, which visually demonstrates how the statistical properties of RETV influence the probabilistic weighting of each estimator over time.

The evaluation criteria described in Section IV.B were computed for the proposed method and the two comparative methods during the LA-92 test, with results summarized in TABLE VI. To provide further insights, the UDDS test was conducted, and all evaluation criteria were recalculated, with the findings presented in TABLE VII.

TABLE VI Evaluation criteria for three SOC estimation scenarios throughout the LA92 test

Method	EKF (7th Polynomial model)	EKF (3rd Gaussian model)	Proposed method
MAX [%]	2.45	2.04	1.79
RMSE [%]	0.8813	0.6718	0.6040
MSE [%]	0.7766	0.4513	0.3648
MAE [%]	0.6547	0.5129	0.4823

TABLE VII Evaluation criteria for three SOC estimation scenarios throughout the UDDS

Method	EKF (7th Polynomial model)	EKF (3rd Gaussian model)	Proposed method
MAX [%]	2.52	3.05	2.49
RMSE [%]	0.9677	0.8079	0.7056
MSE [%]	0.9365	0.6526	0.4815
MAE [%]	0.7621	0.5810	0.4978

TABLE VIII Impact of L_m Values on SoC Estimation RMS and Average Computation Time

Lm	SOC RMSE [%]	Average computation time [s]
100	0.6043	1.8598
200	0.6042	1.8814
300	0.604	1.9072
400	0.6038	1.9309
500	0.6038	1.9529
600	0.6038	1.9704

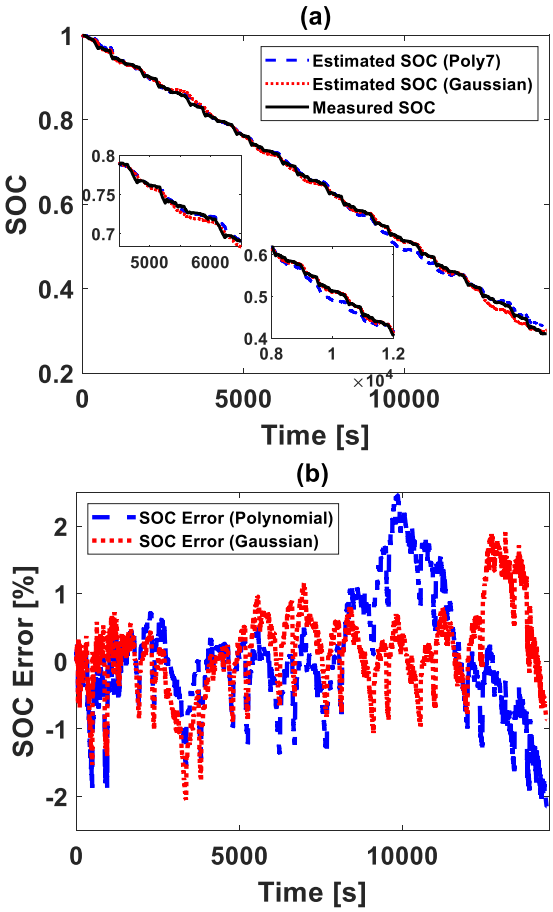

Fig. 6. Comparison of SOC Estimation and Error Using Polynomial and Gaussian Models During LA92. Figure (a) displays the SOC over the test cycle, comparing measured values with estimates from the Polynomial and Gaussian models. The two inset graphs zoom into specific time intervals (5000–6000 s and 8000–12000 s), illustrating regions where each method shows distinct performance characteristics—neither consistently outperforming the other. Figure (b) presents the corresponding SOC estimation error over time for both methods. The error fluctuates throughout the time span, indicating that each approach has its own strengths and limitations depending on the time segment.

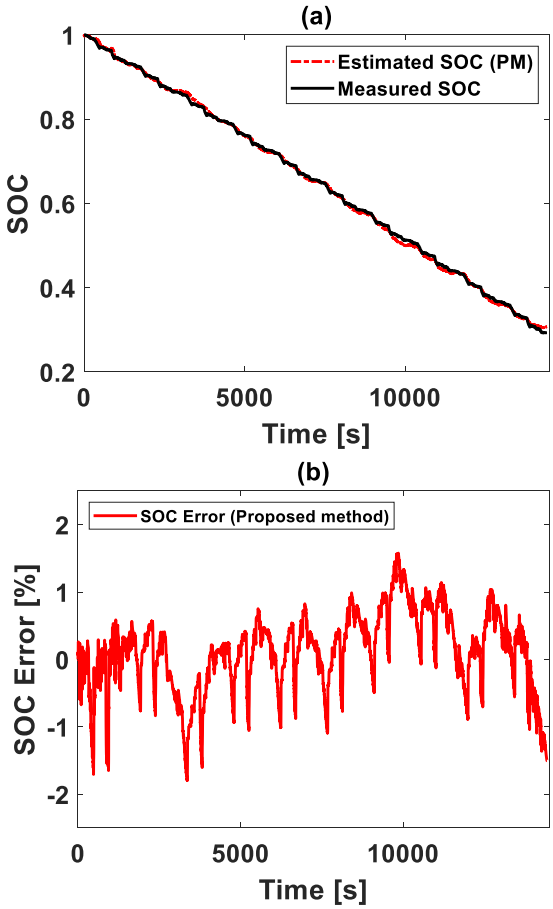

Fig .7. SOC Estimation and Error Using the Proposed Method During LA92 Cycle. shows the estimated SOC using the proposed method (PM) compared against measured SOC over time, demonstrating close alignment between the two curves. Figure (b) presents the corresponding SOC estimation error over time. The error fluctuates between approximately −1.79% and 1.79%, reflecting the dynamic accuracy of the proposed method throughout the test duration.

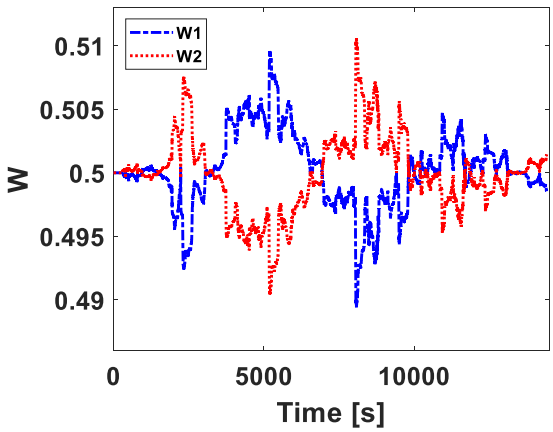

Fig. 8. Dynamic Weights Derived from the Multi-Model Fusion Approach. These dynamic weights reflect changes in system characteristics, as determined by the fusion strategy.

According to Table VI, the proposed method achieves a MAX of 1.79%, representing a 27% reduction compared to the EKF with the 7th-order polynomial model and a 13% reduction compared to the EKF with the 3rd-order Gaussian model. This improvement significantly enhances the reliability of SOC estimation. Furthermore, the proposed method yields an RMSE of 0.6043%, which is approximately 10% lower than the best results of the comparative methods, along with an MSE of 0.3652%, demonstrating superior robustness. The MAE of 0.4827% further confirms the high estimation accuracy throughout the LA92 test.

The UDDS test results, presented in Table VII, reinforce these findings. The proposed method consistently outperforms the other two approaches across all evaluation criteria, confirming its enhanced accuracy, reliability, and robustness under dynamic operating conditions. Notably, these results were obtained under rigorous test scenarios designed to simulate real-world battery behavior, including fluctuating loads and environmental variations. While simpler conditions would likely yield even better performance, the dynamic tests underscore the method's effectiveness in challenging environments. For broader context and comparison, Table VII also includes key benchmarks from existing literature, highlighting the competitive edge of the proposed approach.

TABLE IX . Main work of six papers related to the topic

Ref	Main estimation algorithm	Parameter identification	Battery type	Validation Profile	Error
[37]	AEKF-ESG	Online	LifePO4/2100 mAH	NEDC	RMSE = 0.79%
[38]	FTME-EKF	Online	Lithium-ion	BJDST	RMSE=0.86 MAE = 0.68 %
[19]	AUKF	Online	NCM 2.2Ah	BJDST	RMSE=0.97% MAE=1.13%
[39]	RB-AEKF	Online	Panasonic 18650 lithium-ion	FUDS	RMSE=1.08%
[40]	IFFRLS-UPF	Online	70 Ah lithium battery	BBDST	RMSE=0.72 MAE=0.63
[41]	Improved FFRLS-EXF	Online	27 Ah LG lithium power battery	DST	MAE=1.39% MAX=2.49

V. Conclusions

This paper presents a fusion-based SOC estimation method that integrates two EKFs, each coupled with a distinct OCV-SOC model, and dynamic weighting determined residual error statistics. By combining the strengths of multiple OCV-SOC models, the proposed approach achieves high accuracy, robustness, and computational efficiency under dynamic operating conditions. The fusion strategy, grounded in Bayesian probability and residual analysis, ensures that the most suitable model contributes more heavily to the final SOC estimate at any given time. This dynamic weighting mechanism enhances the adaptability of the framework, allowing it to maintain optimal performance across diverse battery conditions and operating profiles. Simulation results from LA92 and UDDS driving cycles demonstrate that the proposed method consistently outperforms conventional EKF approaches, reducing maximum estimation error by up to 26% and RMSE by over 10%. These improvements validate the effectiveness of the fusion strategy in enhancing SOC tracking precision, even under challenging load profiles.

The method's simplicity and adaptability make it highly suitable for real-time battery management systems in electric vehicles and energy storage applications. Future work may extend this framework to include state-of-health (SOH) estimation and investigate its performance under temperature variations and battery aging effects.

References

[1] A. Degla, M. Chikh, M. Mzir, and Y. Belabed, "State of charge estimation for Li-ion battery based intelligent algorithms," *Electrical Engineering*, vol. 105, no. 2, pp. 1179–1197, Apr. 2023, doi: 10.1007/S00202-022-01728-9/METRICS.

[2] Z. Wei, D. Zhao, H. He, W. Cao, and G. Dong, "A noise-tolerant model parameterization method for lithium-ion battery management system," *Appl Energy*, vol. 268, p. 114932, Jun. 2020, doi: 10.1016/J.APENERGY.2020.114932.

[3] L. Shen, J. Li, J. Liu, L. Zhu, and H. T. Shen, "Temperature Adaptive Transfer Network for Cross-Domain State-of-Charge Estimation of Li-Ion Batteries," *IEEE Trans Power Electron*, vol. 38, no. 3, pp. 3857–3869, Mar. 2023, doi: 10.1109/TPEL.2022.3220760.

[4] C. S. Huang, "A Lithium-Ion Batteries Fault Diagnosis Method for Accurate Coulomb Counting State-of-Charge Estimation," *Journal of Electrical Engineering and Technology*, vol. 19, no. 1, pp. 433–442, Jan. 2024, doi: 10.1007/S42835-023-01533-9/METRICS.

[5] S. Yang *et al.*, "A parameter adaptive method for state of charge estimation of lithium-ion batteries with an improved extended Kalman filter," *Scientific Reports 2021 11:1*, vol. 11, no. 1, pp. 1–15, Mar. 2021, doi: 10.1038/s41598-021-84729-1.

[6] R. Havangi and F. Karimi, "Improvement of The Battery State of Charge Estimation Using Recursive Least Square Based Adaptive Extended Kalman Filter ," *International Journal of Industrial Electronics Control and Optimization*, vol. 7, no. 2, pp. 141–151, May 2024, doi: 10.22111/IECO.2024.47863.1537.

[7] K. Li, X. Gao, C. Liu, C. Chang, and X. Li, "A novel Co-estimation framework of state-of-charge, state-of-power and capacity for lithium-ion batteries using multi-parameters fusion method," *Energy*, vol. 269, p. 126820, Apr. 2023, doi: 10.1016/J.ENERGY.2023.126820.

[8] S. Rout and S. Das, "A robust modified adaptive extended Kalman filter for state- of-charge estimation of

rechargeable battery under dynamic operating condition," *Electrical Engineering*, pp. 1–20, Jun. 2024, doi: 10.1007/S00202-024-02523-4/METRICS.

[9] E. Chemali, P. J. Kollmeyer, M. Preindl, R. Ahmed, and A. Emadi, "Long Short-Term Memory Networks for Accurate State-of-Charge Estimation of Li-ion Batteries," *IEEE Transactions on Industrial Electronics*, vol. 65, no. 8, pp. 6730–6739, Aug. 2018, doi: 10.1109/TIE.2017.2787586.

[10] C. Vidal *et al.*, "Hybrid Energy Storage System State-Of-Charge Estimation Using Artificial Neural Network for Micro-Hybrid Applications," *2018 IEEE Transportation and Electrification Conference and Expo, ITEC 2018*, pp. 868–873, Aug. 2018, doi: 10.1109/ITEC.2018.8450251.

[11] J. Meng, G. Luo, and F. Gao, "Lithium polymer battery state-of-charge estimation based on adaptive unscented kalman filter and support vector machine," *IEEE Trans Power Electron*, vol. 31, no. 3, pp. 2226–2238, Mar. 2016, doi: 10.1109/TPEL.2015.2439578.

[12] H. Pan, Z. Lü, W. Lin, J. Li, and L. Chen, "State of charge estimation of lithium-ion batteries using a grey extended Kalman filter and a novel open-circuit voltage model," *Energy*, vol. 138, pp. 764–775, Nov. 2017, doi: 10.1016/J.ENERGY.2017.07.099.

[13] Y. Tian, B. Xia, W. Sun, Z. Xu, and W. Zheng, "A modified model based state of charge estimation of power lithium-ion batteries using unscented Kalman filter," *J Power Sources*, vol. 270, pp. 619–626, Dec. 2014, doi: 10.1016/J.JPOWSOUR.2014.07.143.

[14] B. Fridholm, M. Nilsson, and T. Wik, "Robustness Comparison of Battery State of Charge Observers for Automotive Applications," *IFAC Proceedings Volumes*, vol. 47, no. 3, pp. 2138–2146, Jan. 2014, doi: 10.3182/20140824-6-ZA-1003.02296.

[15] P. Shrivastava, T. K. Soon, M. Y. I. Bin Idris, and S. Mekhilef, "Overview of model-based online state-of-charge estimation using Kalman filter family for lithium-ion batteries," *Renewable and Sustainable Energy Reviews*, vol. 113, p. 109233, Oct. 2019, doi: 10.1016/J.RSER.2019.06.040.

[16] J. Wu, D. Lei, Z. Liu, and Y. Zhang, "A fusion algorithm of multidimensional element space mapping architecture for SOC estimation of lithium-ion batteries under dynamic operating conditions," *Energy*, vol. 311, p. 133467, Dec. 2024, doi: 10.1016/J.ENERGY.2024.133467.

[17] X. Cheng, X. Liu, X. Li, and Q. Yu, "An intelligent fusion estimation method for state of charge estimation of lithium-ion batteries," *Energy*, vol. 286, p. 129462, Jan. 2024, doi: 10.1016/J.ENERGY.2023.129462.

[18] H. Zhou, J. Luo, and Z. Yu, "Co-estimation of SOC and SOH for Li-ion battery based on MIEKPF-EKPF fusion algorithm," *Energy Reports*, vol. 10, pp. 4420–4428, Nov. 2023, doi: 10.1016/J.EGYR.2023.11.017.

[19] J. Li, M. Ye, X. Ma, Q. Wang, and Y. Wang, "SOC estimation and fault diagnosis framework of battery based on multi-model fusion modeling," *J Energy Storage*, vol. 65, p. 107296, Aug. 2023, doi: 10.1016/J.EST.2023.107296.

[20] Y. Chen, W. Duan, X. Huang, and S. Wang, "Multi-output fusion SOC and SOE estimation algorithm based on deep network migration," *Energy*, vol. 308, p. 133032, Nov. 2024, doi: 10.1016/J.ENERGY.2024.133032.

[21] R. Zhang *et al.*, "A Study on the Open Circuit Voltage and State of Charge Characterization of High Capacity Lithium-Ion Battery Under Different Temperature," *Energies 2018, Vol. 11, Page 2408*, vol. 11, no. 9, p. 2408, Sep. 2018, doi: 10.3390/EN11092408.

[22] I. Baccouche, S. Jemmali, B. Manai, N. Omar, and N. Essoukri Ben Amara, "Improved OCV Model of a Li-Ion NMC Battery for Online SOC Estimation Using the Extended Kalman Filter," *Energies 2017, Vol. 10, Page 764*, vol. 10, no. 6, p. 764, May 2017, doi: 10.3390/EN10060764.

[23] Q. Wang, J. Wang, P. Zhao, J. Kang, F. Yan, and C. Du, "Correlation between the model accuracy and model-based SOC estimation," *Electrochim Acta*, vol. 228, pp. 146–159, Feb. 2017, doi: 10.1016/J.ELECTACTA.2017.01.057.

[24] M. Cacciato, G. Nobile, G. Scarcella, and G. Scelba, "Real-Time Model-Based Estimation of SOC and SOH for Energy Storage Systems," *IEEE Trans Power Electron*, vol. 32, no. 1, pp. 794–803, Jan. 2017, doi: 10.1109/TPEL.2016.2535321.

[25] L. Ren, J. Dong, X. Wang, Z. Meng, L. Zhao, and M. J. Deen, "A Data-Driven Auto-CNN-LSTM Prediction Model for Lithium-Ion Battery Remaining Useful Life," *IEEE Trans Industr Inform*, vol. 17, no. 5, pp. 3478–3487, May 2021, doi: 10.1109/TII.2020.3008223.

[26] Q. Zhang, D. Wang, B. Yang, X. Cui, and X. Li, "Electrochemical model of lithium-ion battery for wide frequency range applications," *Electrochim Acta*, vol. 343, p. 136094, May 2020, doi: 10.1016/J.ELECTACTA.2020.136094.

[27] Y. Wang *et al.*, "A comprehensive review of battery modeling and state estimation approaches for advanced battery management systems," *Renewable and Sustainable Energy Reviews*, vol. 131, p. 110015, Oct. 2020, doi: 10.1016/J.RSER.2020.110015.

[28] X. Lai, Y. Zheng, and T. Sun, "A comparative study of different equivalent circuit models for estimating state-of-charge of lithium-ion batteries," *Electrochim Acta*, vol. 259, pp. 566–577, Jan. 2018, doi: 10.1016/J.ELECTACTA.2017.10.153.

[29] M. R. Ramezani-al and M. Moodi, "A novel combined online method for SOC estimation of a Li-Ion battery with practical and industrial considerations," *J Energy Storage*, vol. 67, p. 107605, Sep. 2023, doi: 10.1016/J.EST.2023.107605.

[30] R. Xiong, Q. Yu, L. Y. Wang, and C. Lin, "A novel method to obtain the open circuit voltage for the state of charge of lithium ion batteries in electric vehicles by using H infinity filter," *Appl Energy*, vol. 207, pp. 346–353, Dec. 2017, doi: 10.1016/J.APENERGY.2017.05.136.

[31] R. Havangi and F. Karimi, "An Adaptive Robust Square Root Unscented Kalman Filter for State of Charge Estimation for Lithium-ion Batteries," *International Journal of Industrial Electronics Control and Optimization*, Jul. 2025, doi: 10.22111/IECO.2025.51512.1679.

[32] P. Shrivastava, T. K. Soon, M. Yamani Bin Idris, and S. Mekhilef, "Lithium-ion Battery Model Parameter Identification Using Modified Adaptive Forgetting Factor-Based Recursive Least Square Algorithm," *Proceedings of the Energy Conversion Congress and Exposition - Asia, ECCE Asia 2021*, pp. 2169–2174, May 2021, doi: 10.1109/ECCE-ASIA49820.2021.9479079.

[33] C. Lin, H. Mu, R. Xiong, and W. Shen, "A novel multi-model probability battery state of charge estimation approach for electric vehicles using H-infinity algorithm," *Appl Energy*, vol. 166, pp. 76–83, Mar. 2016, doi: 10.1016/J.APENERGY.2016.01.010.

[34] S. Sundaresan, B. C. Devabattini, P. Kumar, K. R. Pattipati, and B. Balasingam, "Tabular Open Circuit Voltage Modelling of Li-Ion Batteries for Robust SOC Estimation," *Energies 2022, Vol. 15, Page 9142*, vol. 15, no. 23, p. 9142, Dec. 2022, doi: 10.3390/EN15239142.

[35] Y. Li, C. Wang, and J. Gong, "A multi-model probability SOC fusion estimation approach using an improved adaptive unscented Kalman filter technique," *Energy*, vol. 141, pp. 1402–1415, Dec. 2017, doi:

10.1016/J.ENERGY.2017.11.079.
[36] P. Kollmeyer and M. Skells, "Turnigy Graphene 5000mAh 65C Li-ion Battery Data," *Mendeley Data*, vol. 1, 2020, doi: 10.17632/4FX8CJPRXM.1.
[37] Y. Ye, Z. Li, J. Lin, and X. Wang, "State-of-charge estimation with adaptive extended Kalman filter and extended stochastic gradient algorithm for lithium-ion batteries," *J Energy Storage*, vol. 47, p. 103611, Mar. 2022, doi: 10.1016/J.EST.2021.103611.
[38] Z. Zhang *et al.*, "State of charge estimation of lithium-ion batteries using a fractional-order multi-dimensional Taylor network with adaptive Kalman filter," *Energy*, vol. 316, p. 134577, Feb. 2025, doi: 10.1016/J.ENERGY.2025.134577.
[39] J. Li, L. Li, Z. Li, Z. Jiang, and J. Gu, "Co-estimation of parameters and state of charge for lithium-ion battery," *Journal of Electroanalytical Chemistry*, vol. 907, p. 116011, Feb. 2022, doi: 10.1016/J.JELECHEM.2022.116011.
[40] X. Hao, S. Wang, Y. Fan, Y. Xie, and C. Fernandez, "An improved forgetting factor recursive least square and unscented particle filtering algorithm for accurate lithium-ion battery state of charge estimation," *J Energy Storage*, vol. 59, p. 106478, Mar. 2023, doi: 10.1016/J.EST.2022.106478.
[41] C. Ge, Y. Zheng, and Y. Yu, "State of charge estimation of lithium-ion battery based on improved forgetting factor recursive least squares-extended Kalman filter joint algorithm," *J Energy Storage*, vol. 55, p. 105474, Nov. 2022, doi: 10.1016/J.EST.2022.105474.

Mohammad Moodi received his B.Sc. degree in Power Engineering from Shahid Rajaee Teacher Training University, Tehran, Iran, in 2019, and his M.Sc. degree in Control Engineering from Quchan University of Technology, Quchan, Iran, in 2022. His master's research focused on state-of-charge estimation algorithms for lithium-ion batteries. He is currently a teacher at a Technical and Vocational high school in Bojnurd, Iran. His research interests include battery management systems, control theory, and energy storage technologies.

Mohamad Reza Ramezani-al received his B.Sc. degree in 1998, his M.Sc. degree in 2002 and Ph.D. degree in 2014, all in Control Engineering from Ferdowsi University of Mashhad, Mashhad, Iran. His doctoral research focused on optimal control of switched linear systems. He is currently an Assistant Professor in the Department of Electrical Engineering, Faculty of Electrical and Computer Engineering, Quchan University of Technology, Quchan, Iran. His main research interests include switched systems, nonlinear control systems, control and tracking problems in autonomous underwater vehicles (AUVs), and application of control and estimation theories in power converters and battery management systems.